AIMS Energy, 12(4): 872–904.
DOI: 10.3934/energy.2024041
Received: 09 March 2024
Revised: 08 July 2024
Accepted: 19 July 2024
Published: 02 August 2024

https://www.aimspress.com/journal/energy

Research article

Ring connected microgrid clusters for improved resiliency in distribution systems with high solar PV penetration

W. E. P. Sampath Ediriweera*, N. W. A. Lidula and R. Samarasinghe

Department of Electrical Engineering, University of Moratuwa, Moratuwa, Sri Lanka

* **Correspondence:** Email: ediriweera.sampath@gmail.com; Tel: +94776809569.

Abstract: A ring-connected microgrid cluster can be formed by connecting geographically closed microgrids for mutual power sharing to increase the system's reliability. Real-time power balance within individual microgrids and power sharing among the microgrids of an islanded microgrid cluster would be challenging during contingencies if they are not properly sized and controlled. We propose a technique to design a ring-connected microgrid cluster that has several distributed energy resources. The amount of power flow via interconnecting cables was decided considering the size of the energy storage of the neighboring microgrids. A control system was designed to minimize the effect of severe transients in the neighboring microgrids in the network. The performance of the proposed technique was verified using a ring-connected microgrid cluster with four microgrids derived based on a real distribution system. The results illustrated that the proposed ring-connected microgrid cluster could maintain the power balance of the networked microgrid during the contingencies of neighboring microgrids, increasing the resiliency of the system compared to the radial and islanded operations.

Keywords: energy management; energy storage; microgrid cluster; reliability; renewable power; resilience

1. Introduction

Penetration of renewable generation is increasing due to the increased awareness of the necessities for sustainable development with the learned negative impacts of global warming and environmental pollution. Microgrid clusters have emerged as a solution for facilitating high penetration of renewable energy sources locally to the distribution network [1,2]. Also, microgrid clustering offers further

advantages such as improved reliability, resiliency, and reduction of operating cost compared to the isolated operation of individual microgrids [1,3,4]. Microgrid cluster forms a physical network to achieve local and global objectives through the interaction between the microgrids, and the main grid. The layout of the microgrid cluster depends on the requirements and agreement among microgrids. Microgrid clusters can be classified into three types based on the layout: 1) Radial connected, 2) ring connected, and 3) mesh connected. In the radial-connected microgrid layout, all the microgrids are connected in parallel to the main grid. The ring layout considers a concept where each microgrid is connected to the adjacent two microgrids in the shape of a ring; and energy and information can be shared between them [5,6]. All microgrids in the cluster are interconnected with each other in the mesh layout, making a complex network [7,8]. In other words, each microgrid is connected to all neighboring microgrids through a power transmission and communication network. Compared to the radial layout, ring and mesh layouts offer better scalability, reliability, and stability due to the comparatively higher interconnections among individual microgrids. However, the control and protection of such systems have become complex [2].

Power distribution systems are vulnerable to extreme disruptions and thus, they become the vulnerable part of the electrical power system leading to brown-outs. A resilient power system can prepare, respond, and recover rapidly from major disturbances due to extreme events such as severe weather and climate changes, and catastrophic man-made incidents. Distribution systems with high penetration of solar PV integration are continually threatened by extreme changes in weather conditions and operational conditions [9]. A microgrid can provide more sustained power supply to local consumers through energy management of the on-site distributed energy resources during extreme events. Furthermore, microgrid clusters allow power sharing among each microgrid to balance the load. Therefore, with interconnections among each other, microgrid clusters present a higher level of resiliency and flexibility during extreme events. Existing resilience enhancement strategies can be divided into two categories: 1) Planning strategies to protect against contingencies and 2) operational strategies to minimize load shedding and improve load restoration. Planning strategies involve sizing of distributed energy resources (DER) and are associated with investment, which makes them cost intensive compared to operational strategies [10].

Economics is the most common criterion considered in the planning and designing of microgrid clusters. Sizing the components of a microgrid cluster is an important requirement for the efficient and economic use of renewable resources. A microgrid cluster during networked operation increases the overall profit with optimally sized network components. In [11], a framework to increase the resilience of the microgrid cluster during the designing stage is presented. The system is derived based on a distribution system. The model is formulated to find the best location to connect DERs in the microgrids to reduce the load shedding of the system during extreme events. However, in this study, microgrids do not have fixed boundaries, and islanded zones upon contingencies are taken as microgrids. Thus, cooperative operation of a networked microgrid cannot be expected. The study presented in [12] proposes a bi-level optimization model to enhance the reliability and resilience of a microgrid cluster considering the optimal sizing of the energy storage system. The model is formulated to maximalize the annual net profit. Reliability and resilience constraints are formulated to ensure resilience operation under extreme fault scenarios. A three-level model is proposed in [10] to analyze the resilience and cost of a microgrid cluster with the optimal sizing of the components. The first level of the model is used to maximize the profit while the second and third levels are used to capture resilience. The study presented in [13] proposes a two-stage procedure to optimally size the

components of an isolated microgrid cluster. In the first stage, components are sized for the optimal operation of each microgrid during their islanded operation. In the second stage, a factor based on the operating reserve and the load profile of each microgrid is used to identify the possible capacity reduction of resources during the network operation. In [14], a three-level model is proposed to size and position mobile storage systems in a radial microgrid cluster to increase system resilience. A genetic algorithm is used to optimally size and locate the energy storage system in each microgrid. The consensus algorithm is used to obtain the power-sharing between microgrids to reduce load shedding. In recent years, multi-objective optimization based on game-theoretic technique has been used to optimize different conflicts in a microgrid cluster [15,16]. A multi-objective problem using Objective Particle Swarm Optimization to minimize the cost and increase the reliability of a mesh-connected microgrid cluster is presented in [15]. The ideal sizes of renewable sources and batteries are selected to facilitate the peer-to-grid (P2G) and peer-to-peer (P2P) energy trading schemes based on a proportional sharing scheme. A game theory-based technique is proposed in [16] to facilitate peer-to-grid (P2G) energy trading combined with a peer-to-peer (P2P) energy trading scheme. Also, the model is optimized to optimally select the size of solar PV, wind, and battery, and achieve the maximum payoff from a microgrid network. In case of extreme events such as faults, the affected microgrid normally disconnects from the network operation [17], and this causes a lack of power availability and transients in the other microgrids in the network. It can lead to challenges in supplying continuous power to customers, and survivability over a long time horizon [18]. Therefore, additional constraints are required during the sizing of the components of each microgrid such as the maximum continuous discharge power of the battery, the capacity of the inverter, the DC link capacitor, and their response time in the energy storage system.

The reported literature discussed above are focused only on sizing the resource(s). As presented in [2], ring-connected operation of a microgrid cluster facilitates energy resources-sharing among microgrids, which improves self-sufficiency and reliability. The consumers in a microgrid cluster therefore, could enjoy uninterrupted power for a comparatively longer time duration even at severe system blackouts caused by natural disasters or system faults. A microgrid experiencing a power deficit can import power from the other microgrids with excess power to meet the demand. This concept of regulating the power flow among the microgrids in a ring or mesh microgrid cluster at the energy management layer is not considered in the reported studies.

Although research on the operational strategies to improve the resilience of ring-connected microgrid clusters is limited, related work on radial microgrid clusters is reported. Studies presented in [19,20] have used the energy stored in the electrical vehicles connected to the microgrids to minimize load shedding during extreme events to increase the resilience of radial microgrid clusters without integrating additional power capacity into the network. The study presented in [21], proposes a three-stage stochastic programming-based approach for resiliency-oriented scheduling of a radial connected microgrid cluster to minimize the operating cost, and uncertainties of the renewable power generation and unintentional islanding are embedded in the model. A bi-level optimization algorithm is proposed in [22] to facilitate the pricing for an islanded microgrid cluster. The model is transformed into single-level mathematical programming with equilibrium constraints (MPEC) using Karush-Kuhn-Tucker (KKT) conditions and different linearization tricks. Uncertainties from renewable power generation and non-flexible generation are integrated. The study presented in [23] presents a stochastic-information gap decision theory (IGDT) formulation for the optimal scheduling of isolated microgrids considering component failure to improve resilience. Uncertainties are

integrated into the model, and IGDTs consider the failure of the components in a robust fashion. In [24], a three-stage bidding strategy is proposed for a microgrid cluster with demand response intensives. Different demand responses are modeled to account for the response fatigue. Risks associated with uncertainties related to inflexible demand and renewable generation are controlled through a risk-aversion factor.

The operational strategies such as pricing, and scheduling discussed above are focused only on cost reduction while considering resilience improvement as a requirement. However, in case of extreme events such as faults, the faulted microgrid is normally disconnected from the network. This could lead to instabilities in a ring-connected microgrid cluster in an isolated operation, if the neighboring microgrids have been importing power from the disconnected microgrid. Situation becomes worse in low-inertia microgrids with high penetration of inverter-based renewable power generation [25]. Control structures at the device level, microgrid level, and cluster level can be effectively used in improving the system resilience and sizing of the distributed energy resources, which is not yet reported.

Therefore, we focus on introducing an operational strategy for system's resiliency improvement in a ring-connected cluster of microgrids with high solar PV penetration. We propose the designing and sizing of a power electronic switch, and its controlling to protect the switch and regulate the power flow among the microgrids in the ring-connected microgrid cluster whereas the studies presented in [15,16] are limited to the sizing of energy resources in each microgrid in the cluster. A microgrid during its network operation faces voltage instabilities during extreme events in the neighboring microgrids and the microgrid itself. Energy storage and its control play an important role in maintaining the voltage. This study considers an energy storage system consisting of two power sources: 1) Battery and 2) super capacitor. Unlike [12,13], which are focused only on the capacity and maximum discharging power of battery storage as design parameters, detailed design of the energy storage system integrating additional design parameters such as: the capacity of the voltage source converter, and size of the DC link capacitor is presented in this paper. An effective control architecture aids in coordinating different aspects of the microgrid cluster operation, including energy management system and voltage/frequency regulation. We propose a two-level distributed control architecture to control the ring-connected microgrid cluster for possible operating scenarios such as ring connected, radial connected, and islanded operation while the studies presented in [21–23] on operational strategies do not offer a complete framework on the control of a ring connected microgrid cluster.

The rest of the paper is organized as follows: In section 2, we present the layout and design details of a ring-connected microgrid cluster. The modeling of energy storage systems and power electronic switches are presented in section 3 and section 4, respectively. In section 5 and section 6, we present the proposed control architecture and resiliency aspects of a microgrid cluster, respectively. The test system and the results are presented in section 7. Finally, we conclude the paper in section 8.

2. Ring-connected microgrid cluster

In the ring layout considered in this study, each microgrid is connected to the adjacent two microgrids in the shape of a ring as shown in Figure 1. Here, MG1, MG2, MG3,...., and MGn represent the microgrids 1, 2, 3,…., and n respectively. Energy and information can be shared between them. To regulate the power flow among the microgrids, bidirectional power electronic switches (SW1, SW2, SW3,...., and SWn) are used as shown in Figure 1. Each microgrid in the cluster consists of distributed

energy resources: solar PV systems, energy storage systems, and diesel generators of different capacities. The sizing of the distributed energy resources is done to get the optimal microgrid configuration considering the islanded operation of individual microgrid with energy balance at minimum net present cost using the HOMER Pro v3.10.3 simulation platform. The net present cost represents the difference between the present value of the sum of all costs over the system's lifetime and the revenue. The total cost accounts for the capital, replacement, fuel, and maintenance costs.

During the islanded operation of each microgrid in the cluster, voltage source converter (VSC) of the energy storage system operates in grid-forming mode, setting the microgrid voltage and frequency while other DERs operate in grid-following mode generating constant active and reactive power values. Therefore, the energy storage system responds to transients during the islanded mode operation to stabilize the system. Also, internal faults can induce transients in neighboring microgrids during power sharing, and lead to instability problems, and malfunctioning of the protection systems. Power electronic switches should maintain the continuous regulated power flow to the neighboring microgrids during a fault until the protection system in the affected microgrid detects the fault. Thus, power electronic switches and energy storage systems are the major components in the microgrid cluster considered during the sizing and designing of resilient networks. Detailed designs of energy storage systems and power electronic switches interconnecting adjacent microgrids are discussed in the following sections.

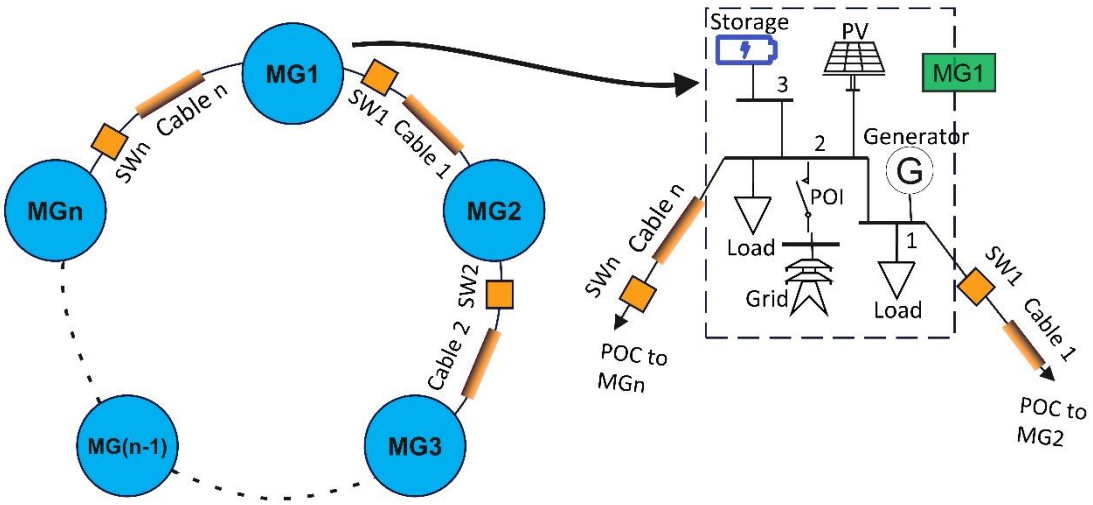

Figure 1. Ring-connected microgrid cluster.

3. Energy storage system

Energy storage system is the main DER in each microgrid. It consists of a VSC, two bidirectional DC-to-DC converters, a battery, a DC link capacitor, a supercapacitor, and a control system as shown in Figure 2. Details of each component is discussed in the following subsections. The VSC is operated in the grid-forming mode during the islanded operation of each microgrid and it is in grid-following mode during the grid-connected operation.

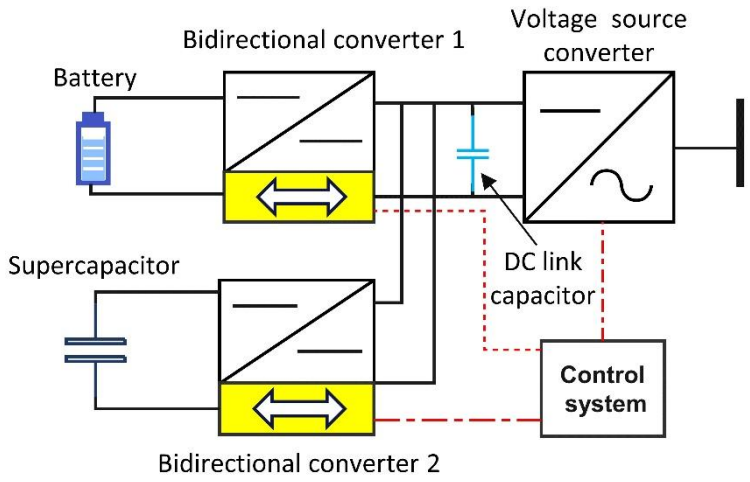

Figure 2. Energy storage system.

3.1. Battery

The battery is considered as the main power source in the energy storage system. A lithium nickel manganese cobalt oxide battery is selected in this study due to its high specific energy values [26]. Currently, lithium-ion batteries are commonly used in power grid applications owing to their higher charge density compared to other rechargeable batteries [27]. The discharging power of the battery is designed to supply the peak load of each microgrid. The maximum charging and discharging power of the battery are considered to be equal. Charging and discharging rates of a battery are usually expressed in terms of C-rate. The performance of the batteries degrades with time during the operation and under rest. There are several external factors affecting the aging of the battery including operating temperature, C-rate, and depth of discharge [28]. High C-rates can charge the battery faster. However, it generates more internal heat and reduces the battery life. Therefore, a balance should be maintained between the charging rate and the lifetime of the battery [29]. This balance influences the rate of charge allowed by the battery management system. Therefore, each battery has an ideal C-rate for the charging and discharging process under standard conditions as recommended by manufacturers [30].

Also, step load changes can occur in microgrids leading to more demand than the total generation capacity of the microgrid including the imported power from the neighboring microgrids. Therefore, it may require load shedding during islanded operation, which compromises the system reliability. Therefore, the battery is allowed to operate beyond the recommended C-rating during such a situation. In the worst-case scenario of operation of the battery beyond the recommended C-rating, overheating of the Li-ion battery may lead to thermal runaway [31]. Thus, the continuous discharge of the battery is limited by the maximum C rate. This limit is usually defined by the battery manufacturer to prevent excessive discharge rates that would damage the battery. Thus, it is ensured that the battery does not discharge current beyond the maximum C-rating. Operating the battery beyond the recommended C-rating can lead to a capacity fade during the operation [27]. Therefore, the recommended discharging power of the battery in i^{th} microgrid ($P_{C,\,rec,\,i}$ [MW]) should be more than the peak load of the microgrid ($P_{L,\,peak,\,i}$ [MW]) as in (1), where, $P_{C,\,max,i}$ [MW] is the discharging power at the maximum C-rating.

$$P_{L,peak,i} \le P_{C,rec,i} < P_{C,\max,i} \; ; i = 1,2...n \tag{1}$$

Also, charging and discharging of the battery and its rates are controlled by the associated bidirectional DC-DC converter (bidirectional converter 1) shown in Figure 2, and its control system is similar to what is proposed in [32].

3.2. Voltage source converter (VSC)

The VSC shown in Figure 2 has a 2-level three-leg converter, LC filter section, and a control system. The control system of the VSC is configured to operate in the grid-forming mode during the islanded operation by setting the microgrid voltage and the frequency, and its control is designed based on [33,34]. It adopts the PQ control mode during the grid-connected operation [35]. The converter is sized to facilitate the power flow when the battery is operating at its maximum discharge rate as given by (2), where $P_{rated\_b,i}$ [MW] is the capacity of the VSC of the energy storage system.

$$P_{rated\_b,i} \ge P_{C,\max,i} \tag{2}$$

The number of inverters connected to microgrids is increasing with high penetration of renewable generation. These inverter-based distributed generation is expected to provide support for the microgrids during the islanded operation. Some of the inverters require semiconductor modules with short-term overload capacity. The high power loss density of power semi-conductors leads to the temperature rise making them incapable of facilitating short-term overload conditions [36]. However, the integration of phase change materials in power semiconductors can reduce the temperature rises and allow the overloads in such cases. According to [36], 3 pu fault current could be facilitated by the VSC for 3 s with the integration of phase change materials. Thus, the maximum transient output power of the converter, $P_{out,\ max,i}$ [MW] can be defined by (3).

$$P_{out,\max,i} = 3 \times P_{rated\_b,i} \tag{3}$$

3.3. Supercapacitor

During the islanded operation of each microgrid, transients such as faults are mainly fed by the grid-forming energy storage system. However, the battery cannot feed fault current beyond its maximum discharging current without damaging the battery. Therefore, as shown in Figure 2, a supercapacitor is connected in parallel with the battery to supply the fault current. Electrochemical double-layer capacitors, also known as supercapacitors, utilize high surface area materials to achieve large capacitance. They also have advantages such as high-power density, long lifespan, low series resistance, and fast charging rates. Therefore, the supercapacitor is sized to supply the fault current for a duration of 3 s. Different supercapacitor models are reported in the literature [37,38]. The widely used RC model is shown in Figure 3(a). Here, R_s [Ω] is the internal resistance, and R_P [Ω] is the self-discharging resistance. However, the typical value for R_P is large and therefore, it can be considered as an open circuit. The simplified RC model shown in Figure 3(b) is considered in this study. In practice, a supercapacitor usually operates between its rated voltage and half of that. Therefore, half of the rated voltage is set as the cutoff voltage

of the supercapacitors considered in this study [39]. Considering negligible internal power losses compared to the power supplied, and constant power consumption (P_c, [MW]), the value of the capacitance of the supercapacitor (C_{sc}, [F]) can be found by (4) [40].

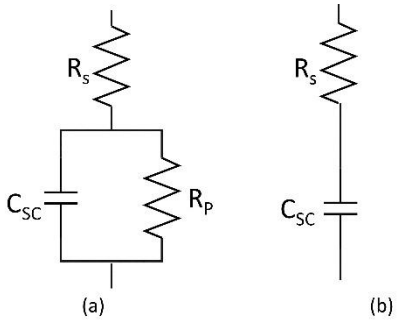

Figure 3. Supercapacitor model.

$$C_{sc} = \frac{2t_{dis}P_c}{(V_0^{\ 2} - V_{cut}^{\ 2})} \tag{4}$$

Here, t_{dis} [s] is discharge duration; V_0 [kV] and V_{cut} [kV] are the rated voltage and cut-off voltage respectively; P_C [MW] is the maximum power supplied by the supercapacitor via the converter, and it is equal to the power given by (3).

3.4. Virtual impedance

During the islanded operation of each microgrid, faults try to draw high fault currents from the grid-forming converters. However, the considered voltage source converter cannot facilitate high over currents than the short-term power rating given by (3). Therefore, a virtual impedance is used to limit the over-current. The idea behind the virtual impedance depends on the physical system's behavior. If the voltage at the terminal of the energy storage system is regulated at the rated value during a fault, then the current fed by the energy storage system increases to an unacceptable value. Therefore, the voltage can be reduced to lower the fault current. Since it is not practical to add a physical impedance to limit the current, a virtual impedance is added by the control system. Virtual impedance (Z, [Ω]) in (5) is triggered only when the current exceeds its nominal value [41].

$$Z = R + jX \tag{5}$$

$$R = \begin{cases} k(I_d - I_{d,ref}), \text{ if } I_d \geq I_{d,ref} \\ 0 \qquad\qquad\quad , \text{ if } I_d < I_{d,ref} \end{cases} \tag{6}$$

$$X = r\sigma_{X/R} \tag{7}$$

Here, R [Ω] defined by (6), and X [Ω] defined by (7) are the resistive component and the reactive components of the virtual impedance, respectively. Parameters, I_d [kA] and $I_{d,ref}$ [kA] are the d-axis

current and the d-axis reference current. The constants, k and $\sigma_{X/R}$ are tuned using the method explained in [42] to limit the current magnitude to a suitable level during an over-current. It should be noted that $I_{d,ref}$ corresponds to the recommended C-rating of the battery, and $I_{d,ref}$ is increased when the battery is operating beyond the recommended C-rating.

Therefore, the voltage set point at the terminal of the energy storage system considering the virtual impedance is given by (8) and (9), where, I_q [kA] and $I_{q,ref}$ [kA] are the q-axis current and q-axis reference current respectively.

$$V_d = V_{d,ref} - I_d R - I_q X \tag{8}$$

$$V_q = V_{q,ref} - I_q R + I_d X \tag{9}$$

3.5. DC link capacitor

The response time of the considered lithium-ion battery storage is 20 ms and the response time of the DC link capacitor is lower than 4 ms [43,44]. Therefore, the DC link capacitor is sized to respond to the transients generated by loads with high ramp rates until the battery comes into full response using (10).

$$C_d = \frac{2.t.p_{step}}{(V_0^{\,2} - V_{\min}^{\,2})} \tag{10}$$

Here, C_d [F] is the capacitance of the DC link capacitor, P_{step} [MW] is the increased load and t [s] is the response time of the battery, and V_0 [kV] is the reference voltage of the DC link. The minimum DC link voltage (V_{min} [kV]) is selected to be higher than the terminal voltage of the fully charged battery.

4. Power electronic switch

A back-to-back bidirectional converter [45,46] is used as the interconnecting switch between two interconnecting microgrids. The structure has a pair of two-level converters beside a DC link as shown in Figure 4.

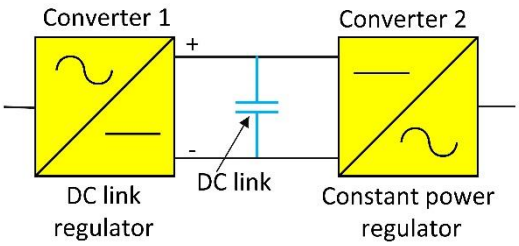

Figure 4. Power electronic switch.

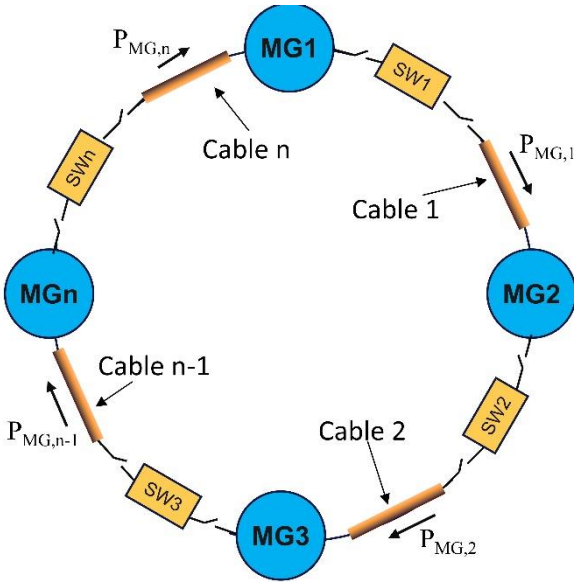

Figure 5. Microgrid cluster.

Converter 1 provides the DC link voltage regulation while converter 2 regulates the active power delivered by it. The control systems adopted in the two converters are similar to the systems proposed in previous studies [35,47]. The converter facilitates the power flow through the interconnection, and provides frequency and voltage support in the case of power deficiency in one of the microgrids provided that the other microgrid has surplus generation/storage available. The connection of the microgrids using back-to-back converters is shown in Figure 5.

Two-level three-phase AC/DC and DC/AC converters have a limitation associated with minimum DC link voltage [48,49]. For the proper operation of the converter with a unity power factor and undistorted current waveforms, the DC link voltage must be maintained above the minimum DC link voltage. Theoretically, the maximum DC link voltage that can be obtained from a diode rectifier (AC/DC converter) is the peak value of the line-to-line voltage ($V_{L\text{-}L}$ [kV]), and it becomes the minimum DC link voltage required in the voltage source rectifier and the inverter [50]. In practical adaptation, the minimum DC link voltage ($V_{DC,\,min}$ [kV]) is slightly more than the theoretical value due to the voltage drop across the filter impedance as illustrated in (11). In practice, the DC link voltage is maintained about 15–20% more than the minimum DC-link voltage [50].

$$V_{DC,\min} = \sqrt{2} \times (V_{L-L} + \text{Voltage drop}) \tag{11}$$

Failure of microgrids during the network operation can lead to stability issues of healthy microgrids during their islanded operation due to sudden surplus/deficit power. During the islanded operation, the energy storage system responds to transients while other distributed energy resources are operating in the grid-following mode.

During the steady state condition, generated power and load in each microgrid are balanced as given by (12), considering negligible power losses. Parameters, P_b [MW], P_s [MW], and P_{gen} [MW] in (12) are the power generated by energy storage, solar PV system, and diesel generator, respectively, while P_L [MW] and P_{Shared} [MW] are the load demand and the power shared with neighboring microgrids.

$$P_b + P_S + P_{gen} = P_L + P_{Shared} \tag{12}$$

During a faulty situation of a microgrid, power sharing may be interrupted, resulting in excess power or deficit power in the neighboring microgrids in the cluster. Therefore, to maintain the energy balance of resulting microgrid clusters, the energy storage should increase its charging or discharging power, which is possible within the safe limits of each energy storage. Thus, the power flowing through each interconnecting cable connected to a microgrid should be maintained to be lower than the reserve capacity of the microgrid. For example, consider the cables 1 and 2 are connected to MG2 in Figure 6. Power flowing through cables 1 and 2 should be lower than the maximum backup power of MG2. This instantaneous backup power is provided by the energy storage system discharging power beyond the recommended C-rating ($P_{C,rec,i}$ [MW]). Backup power compensates for the sudden surplus/deficit power in a healthy microgrid upon failures of the neighboring microgrids. Therefore, power flow via each interconnecting cable connected to the ith microgrid should satisfy (13).

$$\begin{aligned} &(\left|P_{MG,i}\right| \text{and} \left|P_{MG,i-1}\right|) \le P_{C,\max,i} - P_{C,rec,i} \ ; \ \text{if } i = 2,3,....n \\ &(\left|P_{MG,i}\right| \text{and} \left|P_{MG,n}\right|) \le P_{C,\max,i} - P_{C,rec,i} \ ; \ \text{if } i = 1 \end{aligned} \tag{13}$$

Here, $|P_{MG,i}|$ [MW] is the magnitude of the power flowing through the interconnecting cable as illustrated in Figure 6.

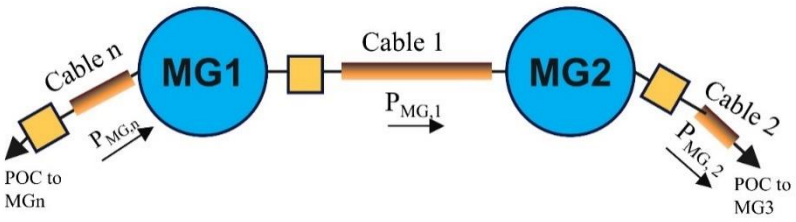

Figure 6. A section of the ring connected microgrid cluster.

Each interconnecting cable is connected to two microgrids during the ring-connected operation. For example, in Figure 6, cable 1 is connected to both MG1 and MG2. By applying (13) separately for MG1 and MG2 (i = 1 and 2) in Figure 6, there are two allowable power-flow through cable 1 ($P_{MG,i}$ [MW] = $P_{MG,i1}$; I = 1 and $M_{PG,i-1}$ [MG] = $P_{MG,i2}$; i = 2). However, power flowing through cable 1 should satisfy the requirements specified by two connected microgrids (MG1 and MG2). Therefore, the maximum allowable power flow through ith cable ($P_{cable,i}$ [MW]) is selected to be the lowest of two values given for the cable as in Eq (14).

$$P_{cable,i} = \min\{P_{MG,i1}, P_{MG,i2}\}; i = 1,2....,n \tag{14}$$

Here, $P_{MG,i1}$ [MW] and $P_{MG,i2}$ [MW] are the two power flow values given by (13) for ith interconnecting cable.

The power electronic switches cannot facilitate short-term overload situations as in transformers. Therefore, each power electronic switch has a maximum current rating it can handle [43]. During disturbances, voltage and frequency in microgrids can experience changes, and therefore current may experience fluctuations while power flowing through the interconnecting cables is being regulated. Thus, current limits associated with converters 1 and 2 in Figure 4 can lead to sudden surplus or deficit power in each microgrid leading to stability problems. Therefore, the power electronic switch should be rated above the maximum allowable power of the connecting cable as given by (15), where, $P_{rated\_SW,\,i}$ [MW] is the rating of ith power electronic switch.

$$P_{rated\_SW,i} > P_{cable,i}\,; i = 1, 2, ..., n \tag{15}$$

4.1. DC link capacitor

During a fault within a microgrid, the DC link voltage of the power electronic switch increases or decreases. Therefore, to protect the DC link capacitor, to avoid the failure of the converters, and to ensure stable operation, the DC link voltage should always be regulated in between the minimum and maximum DC link voltage threshold. To achieve this, upon the detection of a fault in a microgrid, the power electronic switches connected to it should be removed from the network within the holdup time. The holdup time can be identified as the time interval the DC link voltage stays within the thresholds in the case the input power fed to DC link either from converter 1 or converter 2 shown in Figure 4 is lost [51,52]. Thus, the protection of each power electronic switch is facilitated within the holdup time by two simultaneous techniques to increase the redundancy, namely,

1) reduction of the power flow through the power electronic switch to zero by the internal control mechanism and
2) operation of the two mechanical breakers on the two sides of the power electronic switch.

The DC link capacitor should therefore be sized to have enough storage capacity to maintain the minimum DC link voltage during this period. According to the two protection techniques stated above, there will be two holdup times given by (16) and (18). According to the IEC 61000-4-11 standard, the minimum holdup time for low voltage converters is in the range of 10 ms to 20 ms [53].

$$t_{hold,1} = t_w + t_p + t_e \tag{16}$$

$$t_e = I / k_r \tag{17}$$

$$t_{hold,2} = t_w + t_p + t_c \tag{18}$$

In this study, it is considered that a protection system based on the transient characteristics of the current and voltage signals is in operation. Therefore, in (16), t_w [s] is the data window size used by the protection system to detect the failure or faults of the microgrid, and t_p [s] is the processing time of the prediction algorithm detecting the failure of the microgrid; t_e [s] is the time taken by the power electronic switch to reduce the flowing current to zero as defined by (17). In (17), I [kA] is the flowing current through the power electronic switch and k_r [kA/s] is the rate of change of current reduction in each converter. Two mechanical breakers on both sides of each power electronic switch communicate

with each other if a fault is detected. The communication delay is t_c [s].

At the design stage of the DC link capacitor, as given in (19), the holdup time (t_{hold} [s]) is taken as the maximum of the two holdup times given by the two techniques ($t_{hold,1}$ [s] and $t_{hold,2}$ [s]). It ensures proper operation of the power electronic switches until the isolation by any of the methods explained above ensuring the redundant operation.

$$t_{hold} = \max\{t_{hold,1}, t_{hold,2}\} \tag{19}$$

However, upon the isolation of the faulty microgrid from the network operation, the healthy microgrids can experience sudden surplus power or deficit power. Then, it increases/decreases the microgrid voltage with the effect of virtual impendence during their islanded operation. In that case, the central energy management system gives the instructions to each energy storage system after a time delay. The time delay depends on the communication latency and the processing speed of the central energy management system of the microgrid cluster. Then, each energy storage operates in the maximum C-rating to compensate for the excess or deficit power.

4.2. Control of the DC link

During a severe transient such as a fault situation in a microgrid connected to the converter 2 (power flow regulator side) of the power electronic switch shown in Figure 4, it can generate fluctuations in the DC link. Then, converter 1 (DC regulator) tries to regulate the DC link voltage by drawing or supplying current from/to the microgrid, which is connected to converter 1. Therefore, it can induce power swings in the healthy microgrid resulting in stability issues. Also, it increases the complexity of the protection system.

Therefore, an adaptive PI controller is proposed for the outer loop of converter 1 of the power electronic switch shown in Figure 4. During the steady state condition of the power flow, DC link voltage is maintained at the nominal value, and the associated error values in control loops are negligible. Therefore, the controller gains are set to achieve a slow response in the converter. However, during a transient such as a fault or a load-shedding situation in a microgrid, the DC link voltage of the power electronic switch experiences a gradual decline or increase, resulting an error between the measured DC link voltage and nominal DC link voltage. Therefore, upon the detection of a DC link voltage error, tuned control gains are applied after waiting for a duration of the holdup time.

5. Control-architecture of the microgrid cluster

A ring connected microgrid cluster involves different operating scenarios in the connected, islanded, or in transition as an autonomous cluster, as individual microgrids or as groups of microgrids. Therefore, a complex control system is necessary for the microgrid cluster to perform aforementioned tasks to manage itself. These tasks can be carried out on different hardware and software platforms. The management of the tasks of the microgrid can be carried out through several layers such as a device layer, local control layer, supervisory control layer, and high-level grid interface layer by defining clear objectives for each layer. In the IEEE Standard for the Specification of Microgrid Controllers [54], operating tasks of a single microgrid are divided into three control layers.

In this study, a two-level distributed control architecture is used to control the ring-connected

microgrid cluster, including the functions related to cluster level as shown in Figure 7. In the primary control layer, voltage and frequency regulation, islanding detection, grid synchronization, protection, and local power management are at the microgrid level. In the secondary control layer, each microgrid shares the information with other microgrids and the distributed network operator to perform optimum power flow and protection coordination. Different states and modes of the microgrid have specific functions to be executed at any time. The IEEE 2030.7-2017 standard covers two steady-state operating states: grid-connected and islanded modes [54]. In this study, three operating states for the microgrid cluster are considered for analysis considering the possible operating scenarios, namely 1) radial operation, 2) ring operation, and 3) islanded operation. Controllers at the microgrid level and cluster level are updated with the operating state during the operation, and control parameters and functions are updated accordingly.

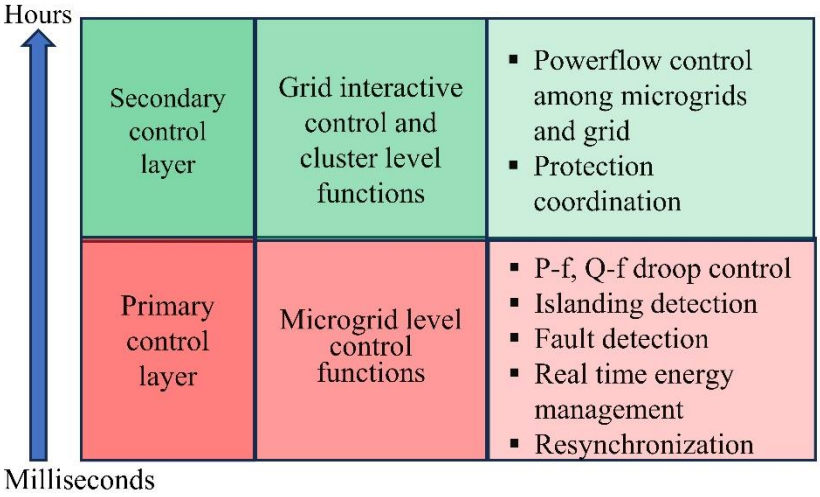

Figure 7. Control architecture.

The microgrid cluster considers the requirements specified in IEEE Standard for "Interconnection and Interoperability of Distributed Energy Resources with Associated Electric Power Systems Interfaces" [55], during the interconnection of the distributed energy resources. The controllers are therefore configured accordingly to maintain the voltage and frequency requirements in response to abnormal conditions [55]. During the islanded operation of each microgrid, the frequency of each microgrid is set by the VSC in the energy storage system.

6. Resilience of the microgrid cluster

Distribution systems are subjected to extreme events due to severe environmental conditions and operational conditions. Therefore, it is necessary to enhance the resilience of the microgrids to avoid long-existing power outages. Quantification of the resilience level of microgrids should be evaluated for the reliable networked operation of microgrids. The performance of a microgrid can be defined considering certain aspects of operation such as power quality, operation security, and generation adequacy. Therefore, the performance can be converted into a quantifiable non-negative value [9,56].

The trapezoid performance function after a severe disturbance in an electrical network is shown in Figure 8, and Q_0 represents the target performance level while $Q(t)$ represents the actual performance

level after a contingency occurring at t_1 [s]. The periods from t_1 [s] to t_2 [s], and t_2 [s] to t_3 [s] are considered as the disaster propagation period, and the post-disaster period, respectively. Also, the period from t_3 [s] to t_4 [s] is the recovery period.

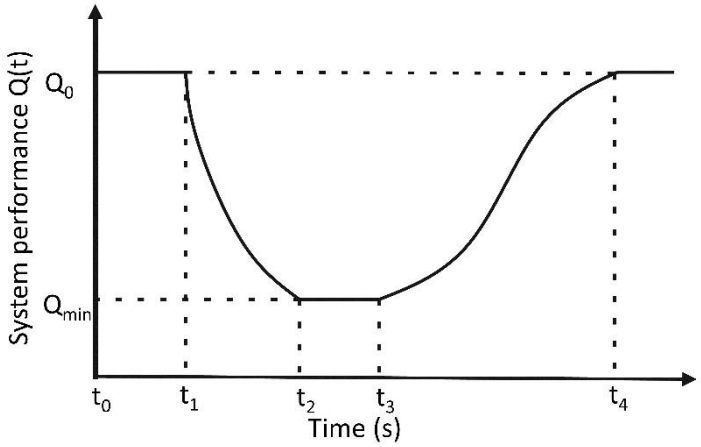

Figure 8. Performance function after a disturbance.

We use the resilience function given by (20) [9], to evaluate the level of resilience of each microgrid in the network after a disturbance.

$$resilience = \frac{1}{loss} \tag{20}$$

The performance "loss" in (20) can be determined by (21) to evaluate the survivability of a microgrid against extreme events. Survivability is a measure of the ability of microgrids to continually deliver essential services during an undesirable event [9].

$$loss_1 = \frac{Q_0 - Q_{\min}}{Q_{\min}} \tag{21}$$

Also, the performance loss can be evaluated more compressively by capturing the degree of robustness, responsiveness to disruptions, and swiftness of recovery. The relative deviation of the performance can be integrated over the duration of performance degradation as given by (22). The degree of robustness measures the degree to which the network is able to withstand an unexpected event without degradation in performance.

$$loss_2 = \int_{t_1}^{t_4} \frac{Q_o - Q(t)}{Q(t)} dt \tag{22}$$

To emphasize the speed of the recovery of the system, the duration of the performance degradation can be included in (22) to get (23).

$$loss_3 = \frac{1}{t_4 - t_1} \int_{t_1}^{t_4} \frac{Q_0 - Q(t)}{Q(t)} dt \tag{23}$$

Thus, Eqs (20) to (23) can be used to quantify the degree of resilience of the microgrids in three different ways and therefore, three resiliency indices can be calculated (RI_1, RI_2, and RI_3). In each case, a value equaling to infinity implies perfect resilience while zero implies no resilience. Here RI_1, RI_2, and RI_3 respectively represent the survivability of a microgrid against extreme events, the degree of robustness, and the speed of the recovery.

7. Result and discussion

A ring connected microgrid cluster with four microgrids was derived using a part of the distribution network in Colombo city, Sri Lanka, as illustrated in Figure 9. Four microgrids, MG1, MG2, MG3, and MG4 in the considered cluster are connected by 11 kV underground cables in a ring. Each microgrid consists of solar PV systems, energy storage systems, and diesel generators of different capacities. The loads in each microgrid are connected through several 11 kV/400 V distribution substations.

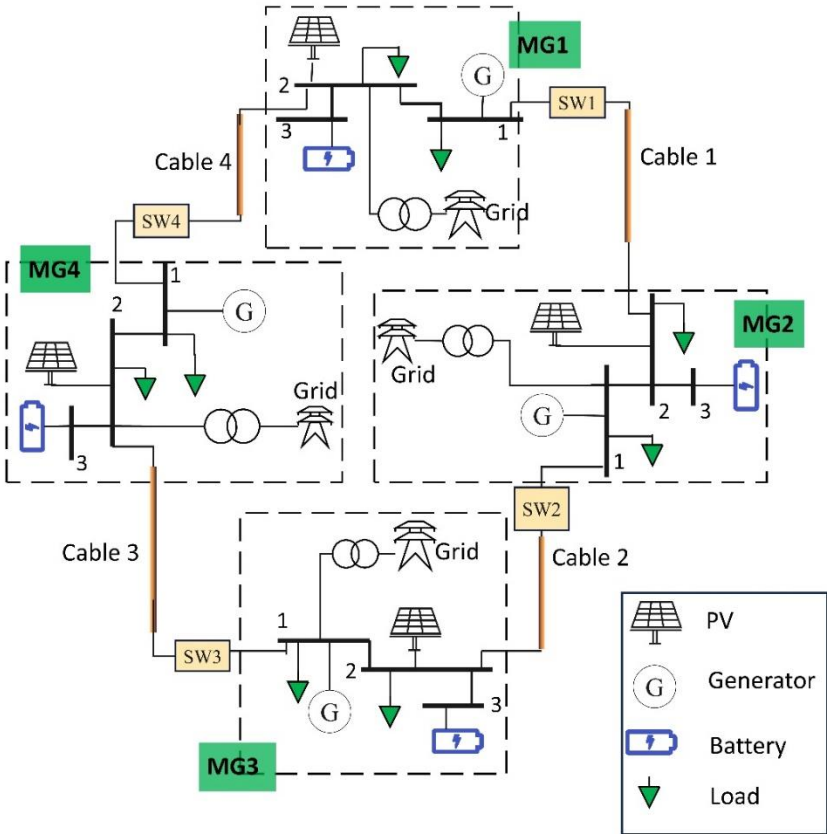

Figure 9. Layout of the microgrid cluster.

Table 1. Loads of the microgrids.

Microgrid	Bus	Active power (kW)	Reactive power (kvar)
MG1	1	2,484	1,203
	2	1,603	776
MG2	1	296	143
	2	289	140
MG3	1	1,452	734
	2	272	137
MG4	1	2,535	1,227
	2	583	282

Table 2. Capacities of the energy resources.

Microgrid	PV (MW)	Battery (kWh)	Diesel generator (MVA)	Load (MVA)
MG1	10.0	21,367	5.100	4.543
MG2	2.2	4,744	0.750	0.651
MG3	10.0	17,070	2.500	1.931
MG4	10.0	24,291	3.900	3.465

Table 1 lists the peak active and reactive load of the selected area observed on 13th December 2021 for 24 hours. Also, the impedances of the cables in each microgrid, and the impedance of the cable interconnecting individual microgrids are listed in the Supplementary (in Table 7).

The capacity of the DERs of the proposed microgrid cluster is listed in Table 2. Also, 14% of the total load at each bus bar is modeled as induction motor loads to match with the percentage of industrial loads in the considered area, and the rest are modeled as static loads. Transformers rated at 10 MVA are used to connect each microgrid to the main grid. The considered network has a low X/R ratio. Also, the effect of power imbalances during the contingencies on frequency drop of microgrids with low X/R ratio is negligible compared to the voltage sag as observed by the authors in their previous studies [57]. Therefore, we focus only on the performance of the voltage profile on the evaluation of the resilient operation.

The proposed ring-connected microgrid cluster and control system are tested on the PSCAD/EMDC v5.01 transient simulation platform. Local energy management proposed by the authors [57,58] is applied in each local microgrid. Central energy management of the cluster is updated with deficit/ excess power in each microgrid via communication, and it facilitates microgrids with excess power to share extra power with microgrids with power deficit. The amount of power received by each microgrid with a power deficit is decided by the central management system. Then, the power flow arrangement among the microgrids is calculated by the central energy management system to facilitate the power-sharing subjected to cable capacity constraints and power losses. The central management system sends command signals to the active power regulator of each power electronic switch to regulate the power flow arrangement among microgrids. The 5G wireless communication system in each microgrid ensures a low latency level of around 1 ms. The parameters given by (1)–(19) are used to design the energy storage system and power electronic switches, and their values are listed in the Supplementary (Table 8). To show the design performance of the microgrid cluster, two case studies were conducted subjecting the test system into contingencies. The DC link voltages of the power electronic switches are regulated within 4 ± 1 kV.

7.1. Case study 1

In case study 1, islanded microgrid cluster with two possible operation configurations; ring and radial are considered initially as shown in Figures 10(a) and 11(a) respectively. It is observable that the cluster operation scenario changes during permanent faults. Some microgrids get individually islanded while some move to different radial operations. Let's consider initial ring operation of the cluster as Case A and initial radial operation of the cluster as Case B.

Both ring and radial networked operations consider the same load and maximum available solar power in each microgrid. The initial load, power generations, and state of charge (SOC) of energy storages in the microgrids during ring and radial operation are listed in Table 3. State of charge levels of each microgrid are more than 30%, and therefore, according to the local energy management system [57], the diesel generators are not in operation in case study 1.

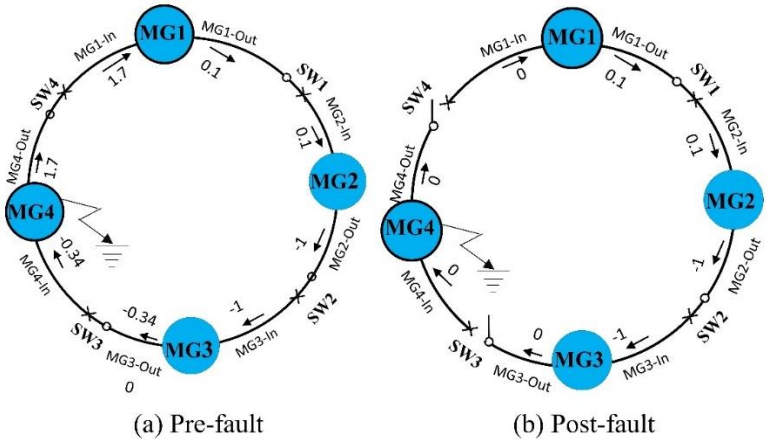

Figure 10. Islanded ring connected microgrid cluster in three possible operation scenarios at a fault.

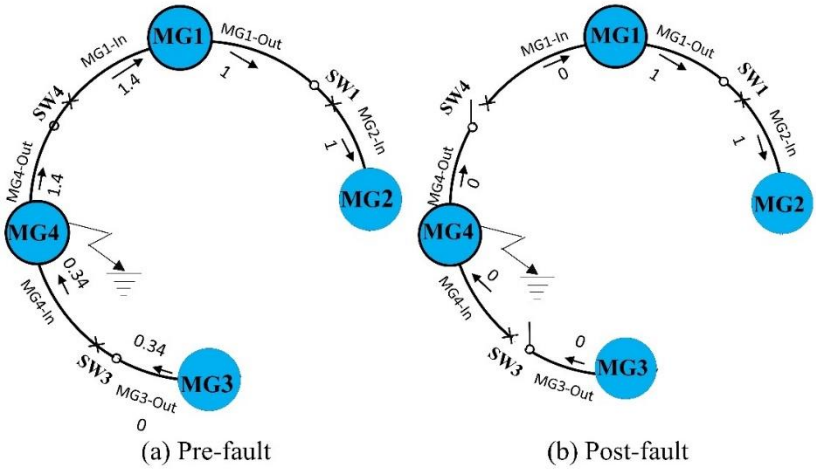

Figure 11. Islanded radial connected microgrid cluster in three possible operation scenarios at a fault.

The MG4 during ring and radial connected configurations shown in Figures 10(a) and 11(a) are subjected to an internal three-phase fault at 2.3 s, respectively. Figures 10(b) and 11(b) illustrate the post-fault layouts of the ring and radial connected configurations, respectively. The operations of two mechanical breakers on the two sides of the power electronic switches are disabled to see the internal operation of the power electronic switches during transients.

Table 3. Setting and changes of microgrids; Case study 1.

Microgrid Cluster Operation Scenario	Energy Resources	Power (MW)			
		MG1	MG2	MG3	MG4
Case A (Initially Ring—Figure 10(a))	Load	6.64	0.58	2.05	2.77
	Solar	0.06	0	5.07	8.31
	Storage	4.9	−0.33	−2.26	−3.50
	Generator	0	0	0	0
	SOC (%)	70	60	50	40
Case B (Initially Radial—Figure 11(a))	Load	6.64	0.58	2.05	2.77
	Solar	0.06	0	4.7	7.33
	Storage	6.28	−0.370	−2.24	1.28
	Generator	0	0	0	0
	SOC (%)	70	60	50	40

Figure 12 illustrates the in, and out power flow of the microgrids MG1, MG2, MG3, and MG4, and the DC link voltage of the power electronic switches during the fault on initial ring operation of the microgrid cluster (Case A), while Figure 13 illustrates the same during initial radial operation of the microgrid cluster (Case B). Figure 14 illustrates the RMS voltage at the terminal of the energy storage of microgrids MG1, MG2, MG3, and MG4 for Case A and Case B.

Case study 1 focuses only on the effect of the internal fault in MG4 on the operation of the rest of the microgrids in the cluster. With the internal three-phase faults occurring at 2.3 s in MG4, the local voltage of MG4 reduces from 1 pu in response to the current drawn by the fault irrespective of the layout of the microgrid cluster as shown in Figure 14. Then, the microgrid cluster goes through several events until the systems come back to the recovery state.

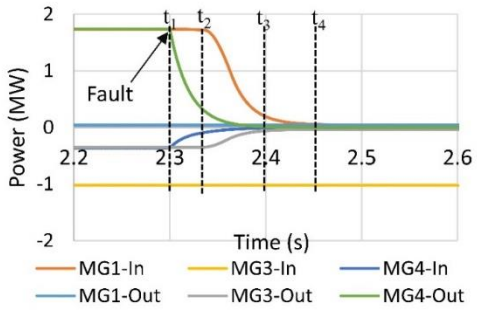

(a) In and out power flow of the microgrids.

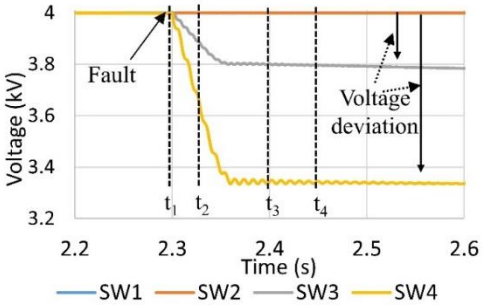

(b) DC link voltage of power electronic switches.

Figure 12. In and out power flow of microgrids and DC link voltage of power electronic switches for Case A.

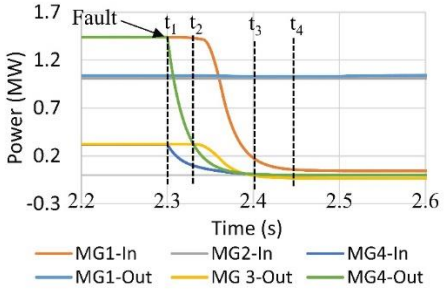

(a) In and out power flow of the microgrids.

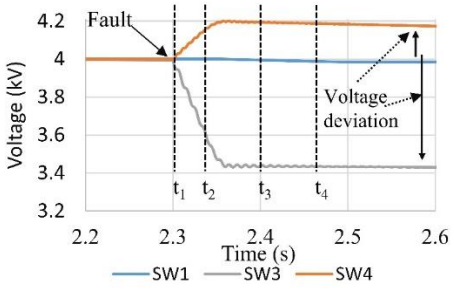

(b) DC link voltage of power electronic switches.

Figure 13. In and out power flow of microgrids and DC link voltages of power electronic switches for Case B.

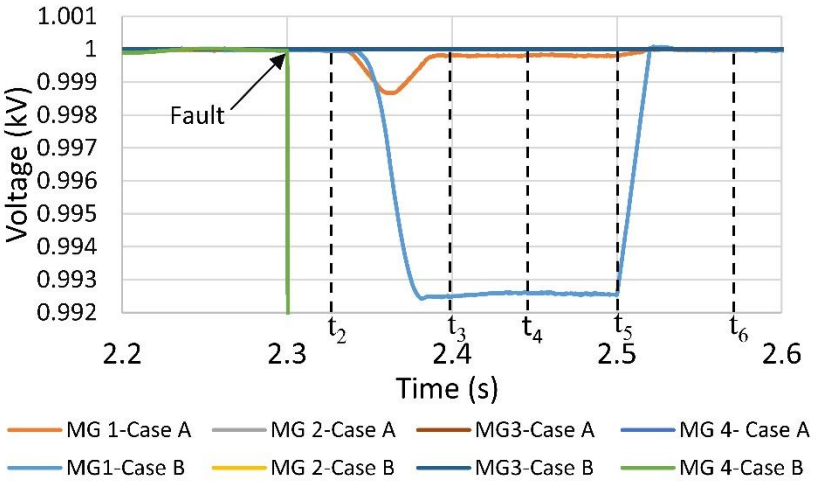

Figure 14. RMS voltage at the terminal of energy storages in microgrids.

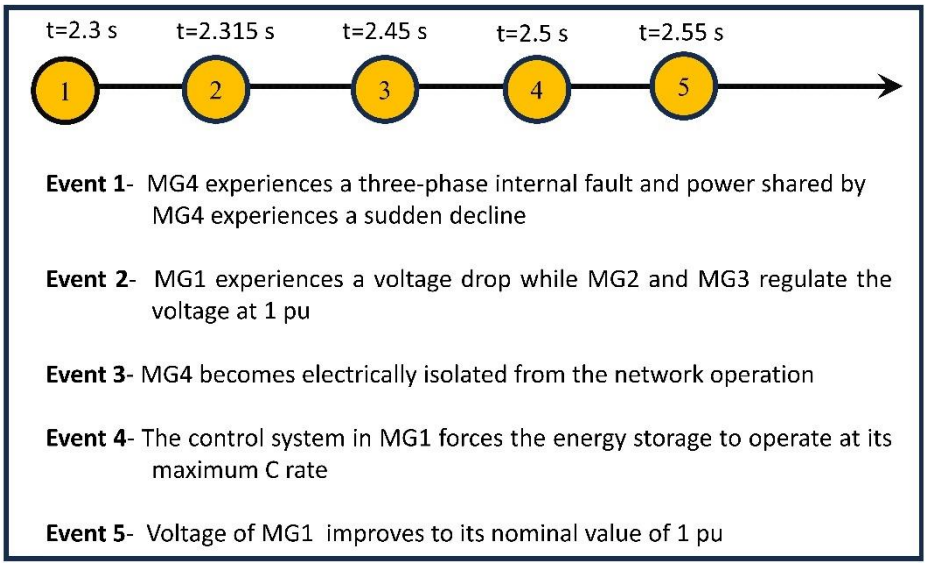

Figure 15. Stages of recovery of microgrid cluster.

The timeline shown in Figure 15 illustrates the events during the recovery stages of the microgrid cluster upon the fault in MG4. The events are explained in the following.

- **Event 1**

As shown in Figures 12(a) and 13(a), once the MG4 experiences the fault at 2.3 s (t_1), power shared by MG4 from/to MG1 and MG3 experiences a sudden decline irrespective of the layout of the microgrid cluster. Therefore, as shown in Figures 12(b) and 13(b), DC link voltages of power electronic switches SW3 and SW4 deviate from 4 kV.

• **Event 2**

According to Figures 12(a) and 13(a), the controls of the power electronic switches are slow enough to continue power flow between SW4 and MG1, and between SW3 and MG3 until the fault is detected by the protection relays and inform the power electronic switches SW4 and SW3 by 2.315 s (t_2). Then, the control system of the power electronic switches reduces the flowing current at a rate of 20 kA/s, and therefore, MG1 experiences a voltage drop as shown in Figure 14 while MG3 maintains the RMS voltage at 1 pu.

• **Event 3**

As shown in Figures 12(a) and 13(a), power flow between SW4 and MG1, and between SW3 and MG3 reduces to zero by 2.45 s (t_4), and thus, MG4 becomes electrically isolated from the network operation. Even though MG1 lost the power imported from MG4, it continuously maintains the power exported to MG2, presented by MG1-Out in Figures 12(a) and 13(a).

• **Event 4**

The fault protection system in MG4 informs MG1, MG2 and MG3 at 2.5 s (t_5) via the central controller of the microgrid cluster regarding the occurrence of the fault. Therefore, the control system in MG1 changes the setting of the energy storage and forces it to operate at its maximum C-rate.

• **Event 5**

The voltage of MG1 again improves to its nominal value of 1 pu by 2.55 s (t_6) as shown in Figure 14. However, MG3 does not experience any power deficit even if it lost 0.34 MW imported from MG4 according to Figure 10, in initial ring connected operation (Case A). Thus, MG3 maintains the RMS voltage at 1 pu while MG1 continues exporting 0.1 MW to MG2 as shown in Figure 10(b). As the pentation level of the solar PV generation in MG1 is at a minimum of 0.06 MW according to Table 3, it does not offer surplus power for power sharing. Also, MG1 keeps on exporting power of 1 MW to MG2 in the post-fault configuration of the radial microgrid cluster (Case B) as shown in Figure 11(b). Therefore, MG1 experiences a power deficit of 0.9 MW if it was in radial cluster operation initially compared to being in ring-connected cluster operation initially.

The voltage drop of MG1 is 0.0005 pu and 0.0075 pu during Case A and Case B operations, respectively, as shown in Figure 14. Therefore, the voltage regulation of MG1 is improved by 93% if it was in the initial ring-connected operation compared to being in radial cluster operation.

The energy storage system of each microgrid responds to transients ensuring the energy balance of each microgrid, and the terminal voltage of the energy storage system is maintained at 1 pu. However, if the total demand is more than the available generation capacity of a particular microgrid including the shared power, then the terminal voltage experiences a sag. Thus, it becomes a measure of power quality and availability of the generation to satisfy the demand. We consider the voltage sag of each microgrid during contingencies to evaluate the resilient operation of the proposed network. Therefore, the voltage curves shown in Figure 14 can be converted to a performance curve as shown in Figure 16.

Since the voltage of the MG2 and MG3 are not affected, their performances are not considered. Since case study 1 investigates the effect of the fault occurring in MG4 on the neighboring microgrids, the performance of MG4 is not evaluated. Levels Q_1 and Q_2 on Figure 16 consider the performance during the post-disaster period of the performance curve of MG1during initially radial and ring connected microgrid cluster operations. Then, the resilient indices given by equations (21) to (23) are used to evaluate the resiliency of MG1, and they are listed in Table 4. The ability of MG1 to continually deliver essential services during an undesirable event (survivability) (RI_1) is 3.7 and 1.35 during initially ring and radial connected microgrid clusters operations, respectively.

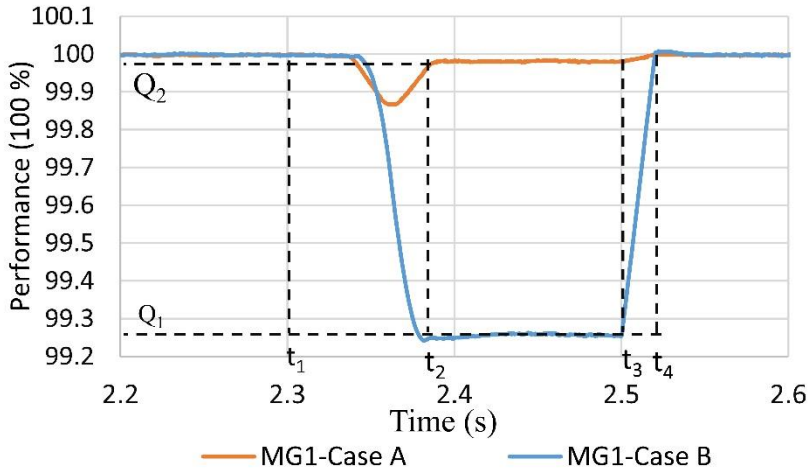

Figure 16. Performance curve of MG1 for initially ring (Case A) and radial (Case B) connected microgrid clusters.

Table 4. Resilience indices of MG1; Case study 1.

Layout	Resiliency indices		
	RI_1 (survivability)	RI_2 (degree of robustness)	RI_3 (speed of recovery)
Case A	3.7	34.72	13.85
Case B	1.35	10.67	4.27

Table 4 presents the calculated resilience indices. The degree to which MG1 is able to withstand an unexpected event without degradation in performance (degree of robustness) (RI_2) is therefore, 34.72 and 10.67 during initially ring and radial connected cluster operations, respectively. Thus, ring-connected operation of the microgrid cluster improves the survivability and the degree of robustness of the MG1 by 170% and 225% respectively compared to the radial operation of the microgrid cluster in the event of a failure of neighboring microgrids during power sharing. Therefore, ring connected operation of microgrid cluster improves the resilience of a single microgrid compared to the radial connected operation of the microgrid cluster in the event of a failure of neighboring microgrids.

During the network operation of microgrids without connections to the main grid, power-sharing among the microgrids occurs through the interconnecting microgrids. During the radial operation,

MG4 shares power with MG2 through MG1 as shown in Figure 11(a). However, during the ring-connected operation, MG1 receives power in two directions as shown in Figure 10(a). Thus, intermediate microgrids may not be able to maintain the local power balance with the isolation of MG4. Therefore, the local voltages experience a drop in response to the local power imbalance. Thereafter, the controllers of the energy storage system come into operation. However, during the recovery period of the microgrids, the voltage at the terminal of the energy storage system (Bus 3) is within the limits specified in IEEE 1547-2018 as shown in Figure 14.

7.2. Case study 2

In case study 2, microgrids in the cluster operate in ring, radial, and islanded operations considering the same load and maximum available solar power in each microgrid as in case study 1. Initial demand, generation, settings, and changes of the microgrids during ring, radial, and islanded operations are listed in Table 6. During the islanded operation, microgrids are not networked, and there is no cooperation and power sharing among the microgrids in the cluster. Also, the islanded operation focuses only on MG1, and thus, parameters of MG2, MG3, and MG4 during the islanded operation are not listed in Table 5. The solar PV system in MG1 is removed at 2.4 s from the network during the operation to simulate a failure of the solar PV system in MG1.

Table 5. Setting and changes of microgrids; Case study 2.

Layout	Energy Resource	Power (MW)			
		MG1	MG2	MG3	MG4
Ring	Load	8.4	0.58	2.05	2.77
	Load shedded	0.7	N/A	N/A	N/A
	Solar	1.89	0	5.07	8.49
	Storage	4.9	−0.33	−2.26	−3.59
	Generator	0	0	0	0
	SOC (%)	70	60	50	40
Radial	Load	8.4	0.58	2.05	2.77
	Load shedded	1.41	0	0	0
	Solar	1.89	0	4.7	7.33
	Storage	6.28	−0.370	−2.24	−3.44
	Generator	0	0	0	0
	SOC (%)	70	60	50	40
Islanded	Load	8.4	N/A	N/A	N/A
	Load shedded	1.93	N/A	N/A	N/A
	Solar	1.89	N/A	N/A	N/A
	Storage	6.54	N/A	N/A	N/A
	Generator	0	N/A	N/A	N/A
	SOC (%)	70	N/A	N/A	N/A

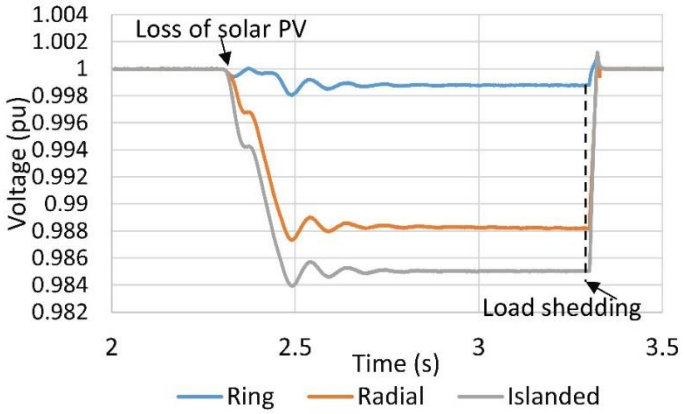

Figure 17. RMS voltage at the terminal of energy storage in MG1.

Figure 17 shows the RMS voltage at the terminal of the energy storage of MG1 during ring, radial, and islanded operations. Also, each local energy management system is responsible for local energy balance during the network operation. Therefore, other microgrids do not experience any contingencies with the power imbalance in MG1, and the power flow arrangement among the microgrids is similar to the power flow arrangement in case study 1 (Figures 10(a) and 11(a)). With the failure of the solar PV system in MG1 at 2.3 s, MG1 experiences a sudden power deficit of 1.89 MW. Therefore, the voltage of MG1 reduces at a ramp in response to the current drawn by the load and the voltage becomes 0.999 pu, 0.989 pu, and 0. 985 pu under ring, radial, and islanded operations, respectively, as shown in Figure 17. Therefore, to maintain the local power balance of MG1, 0.7 MW, 1.4 MW, and 1.93 MW of loads are shedded during its ring, radial, and islanded operation at 3.3 s as listed in Table 5. Then, the voltage at the terminal of the energy storage in MG1 comes back to 1 pu. The radial operation reduces the load shedding by 26% compared to the islanded operation while the ring-connected operation has reduced the load shedding by 50% compared to that of radial operation.

Table 6. Resiliency indices; Case study 2.

Layout	Resiliency Indices		
	RI_1 (survivability)	RI_2 (degree of robustness)	RI_3 (speed of recovery)
Ring	5.55	9.12	9.12
Radial	0.81	0.92	0.92
Islanded operation	0.63	0.71	0.71

Resiliency indices of the MG1 are listed in Table 6. In MG1 during islanded operation, 22.5% of the load is supplied by solar PV generation. Due to the sudden loss of the generation and with the unavailability of rotating masses, the voltage experiences a sag due to power imbalance. Thus, the survivability (RI_1) and the degree of robustness (RI_2) of the MG1 under loss of solar PV system are 0.631 and 0.71, respectively, during the islanded operation. The ring-connected operation of the microgrid cluster improves the ability of MG1 in continually delivering essential services during an undesirable event by 58% and 77%, respectively, compared to the radial and islanded operation of the

microgrid cluster in the event of a failure of the solar PV system during power sharing. Also, ring-connected operation enhances the degree to which MG1 is able to withstand an unexpected event without degradation in performance by 89% and 118% compared to radial and isolated operations respectively.

Ring-connected operation improves the survivability of MG1 (RI_1) by 170% and 58% during case studies 1 and 2 compared to radial e operation of microgrid clusters. Also, the degree of robustness (RI_2) is improved by 225% and 89% compared to radia operation. Thus, the resilience of operation of networked operations can be improved by configuring the network in a ring rather than radial and islanded operations.

In case of a blackout caused by man-made or natural disasters, the ring-connected operation of the micirgrid cluster can facilitate power-sharing among microgrids and it supports the consumers over a long time horizon, probably until the grid is restored. The voltage of microgrids with a low X/R ratio is subjected to fluctuation during power imbalance in microgrids when they are not connected to the main grid. In case of extreme events such as faults, the affected microgrid experiences a significant voltage drop as illustrated in case study 1. Therefore, it is no longer capable of sharing power. However, with the proposed adaptive PI controller, power electronic switches maintain continuous power flow to the neighboring microgrids, discharging or charging the DC link capacitors of the power electronic switches until the protection system detects and removes the faulty microgrid from the network operation. With the support of the properly sized DC link capacitor in the energy storage system, the batteries in the neighboring microgrids come to its full response to support the sudden loss of shared power. The isolated microgrid informs the neighboring microgrids regarding the occurrence of the fault via the central controller. Therefore, the battery can operate at its maximum C-rate if the microgrid experiences a power deficit. With the proper sizing of the energy storage system, power electronic switch, and properly defined control architecture, none of the neighboring microgrids experience reliability issues due to extreme events. Therefore, ring-connected operation offers improved resilience of the microgrids against extreme events occurring in neighboring microgrids during its network operation compared to the radial-connected operation.

Adverse weather conditions affect renewable power generation. During a sudden loss of renewable power generation in a microgrid as explained in case study 2, the available total generation is not enough to support the loads without the grid support, and the voltage of the microgrid is reduced by the grid-forming inverter. Then, the load shedding scheme sheds a minimum amount of load to maintain the energy balance. The microgrid experiencing a power deficit can get the power from the cluster in two different connections during ring-connected operation. Therefore, the ring-connected operation offers improved reliability reducing the amount of load shedded compared to the radial and islanded operation. Thus, the ring-connected operation of the proposed microgrid cluster can significantly improve the resilience and reliability of the microgrid during an extreme event such as loss of renewable power generation compared to the radial operation and islanded operations of microgrids.

8. Conclusions

We propose a technique to design and control a ring-connected microgrid cluster with high penetration of renewable power generation to increase the resiliency during contingencies. At the microgrid level, the design focus was on the energy storage system and its control. At the cluster level,

a power electronic switch was designed to share the surplus power available in the cluster among the microgrids with the power deficit. The design and control system were adopted for a ring-connected four microgrids derived based on a real distribution system and accurate operation was validated through simulations on PSCAD/EMTDC v5.0.1. Two case studies were presented based on two extreme events to verify the improved resilience of the proposed ring-connected microgrid cluster compared to the radial-connected configuration and islanded operation. The following are the specific conclusions drawn from the study:

- The control tasks defined in IEEE 2030.7-2017 standard were successfully adopted for implementing the objectives of the ring connected microgrid cluster on power sharing and coordination of the power electronics interface among microgrids allowing different operating modes of the network operation.
- Ring networked operation of microgrids reduces the performance loss of microgrids improving the ability to continuously deliver power to the consumers against extreme events by more than 58%, and the degree to which the microgrid is able to withstand disruptions, by more than 89% compared to the radial operation for the considered case studies.
- Networked operation of microgrids allows the sharing of power among them to support microgrids in a power deficit. However, failure of microgrids during power sharing can lead to sudden power deficit of intermediate microgrids in the network leading to power imbalances and reliability issues. With the proposed design and the control of the microgrid cluster during ring networked operation maintained the voltage profile of the affected microgrids within limits specified in IEEE 1547-2018 while improving the resilience level by more than 58% compared to the radial operation.

Renewable sources-based distributed generation connected to the distribution network cannot be controlled effectively with the lack of control and operation flexibility during a blackout caused by natural or man-made disasters. In case of a blackout, each microgrid in the proposed system with its energy storage system can operate in an islanded operation to support the customers until the grid is restored. The ring-connected operation of the microgrid cluster facilitates power-sharing among microgrids. Thus, the microgrid experiencing a power deficit can get the power from the microgrids having excess power to support consumers. Thus, the proposed ring-connected microgrid cluster with proper design and controls, can significantly improve the resilience and reliability compared to the radial operation and islanded operations of microgrids.

Use of AI tools declaration

The authors declare they have not used Artificial Intelligence (AI) tools in the creation of this article.

Acknowledgments

The authors gratefully acknowledge the support provided by the Senate Research Committee University of Moratuwa; Grant number SRC/LT/2020/33 and Manitoba Hydro International by giving the PSCAD professional license.

Conflict of interest

The authors declare no conflicts of interest.

Author contributions

Conceptualization, W. E. P. S. Ediriweera and N. W. A. Lidula; methodology, W. E. P. S. Ediriweera; software, W. E. P. S. Ediriweera; validation, W. E. P. S. Ediriweera; formal analysis, W. E. P. S. Ediriweera, and N. W. A. Lidula; investigation, W. E. P. S. Ediriweera; writing—original draft preparation, W. E. P. S. Ediriweera; writing—review and editing, W. E. P. S. Ediriweera, N. W. A. Lidula, and R. Samarasinghe; visualization, W. E. P. S. Ediriweera, N. W. A. Lidula, and R. Samarasinghe; supervision, N. W. A. Lidula; project administration, N. W. A. Lidula. All authors have read and agreed to the submitted version of the manuscript.

References

1. Xu Z, Yang P, Zheng C, et al. (2018) Analysis on the organization and development of multi-microgrids. *Renewable Sustainable Energy Rev* 81: 2204–2216. https://doi.org/10.1016/j.rser.2017.06.032
2. Ediriweera WEPS, Lidula NWA (2022) Design and protection of microgrid clusters: A comprehensive review. *AIMS Energy* 10: 375–411. https://doi.org/10.3934/energy.2022020
3. Saleh MS, Althaibani A, Esa Y, et al. (2015) Impact of clustering microgrids on their stability and resilience during blackouts. *2015 International Conference on Smart Grid and Clean Energy Technologies (ICSGCE)*, 195–200. https://doi.org/10.1109/ICSGCE.2015.7454295
4. Hossain MJ, Mahmud MA, Milano F, et al. (2015) Design of robust distributed control for interconnected microgrids. *IEEE Trans Smart Grid* 7: 2724–2735. https://doi.org/10.1109/TSG.2015.2502618
5. John T, Lam SP (2017) Voltage and frequency control during microgrid islanding in a multi-area multi-microgrid system. *IET Gener Transm Dis* 11: 1502–1512. https://doi.org/10.1049/iet-gtd.2016.1113
6. Liu T (2018) Energy management of cooperative microgrids: A distributed optimization approach. *Int J Electr Power Energy Syst* 96: 335–346. https://doi.org/10.1016/j.ijepes.2017.10.021
7. Choobineh M, Silva-Ortiz D, Mohagheghi S (2018) An automation scheme for emergency operation of a multi-microgrid industrial park. *IEEE Trans Ind Appl* 54: 6450–6459. https://doi.org/10.1109/TIA.2018.2851210
8. Gregoratti D, Matamoros J (2015) Distributed energy trading: The multiple-microgrid case. *IEEE Trans Ind Electron* 62: 2551–2559. https://doi.org/10.1109/TIE.2014.2352592
9. Li Z, Shahidehpour M, Aminifar F, et al. (2017) Networked microgrids for enhancing the power system resilience. *Proc IEEE* 105: 1289–1310. https://doi.org/10.1109/JPROC.2017.2685558
10. Wang Y, Rousis AO, Strbac G (2021) A three-level planning model for optimal sizing of networked microgrids considering a trade-off between resilience and cost. *IEEE Trans Power Syst* 36: 5657–5669. https://doi.org/10.1109/TPWRS.2021.3076128

11. Baghbanzadeh D, Salehi J, Gazijahani FS, et al. (2021) Resilience improvement of multi-microgrid distribution networks using distributed generation. *Sustainable Energy Grids Netw* 27: 100503. https://doi.org/10.1016/j.segan.2021.100503
12. Xie H, Teng X, Xu Y, et al. (2019) Optimal energy storage sizing for networked microgrids considering reliability and resilience. *IEEE Access* 7: 86336–86348. https://doi.org/10.1109/ACCESS.2019.2922994
13. Salehi N, Martínez-García H, Velasco-Quesada G (2022) Component sizing of an isolated networked hybrid microgrid based on operating reserve analysis. *Energies* 15: 17. https://doi.org/10.3390/en15176259
14. Wang Y, Rousis AO, Strbac G (2022) Resilience-driven optimal sizing and pre-positioning of mobile energy storage systems in decentralized networked microgrids. *Appl Energy* 305: 117921. https://doi.org/10.1016/j.apenergy.2021.117921
15. Lokesh V, Badar AQH (2023) Optimal sizing of res and bess in networked microgrids based on proportional peer-to-peer and peer-to-grid energy trading. *Energy Storage* 5: 464. https://doi.org/10.1002/est2.464
16. Ali L, Muyeen SM, Ghosh A, et al. (2020) Optimal sizing of networked microgrid using game theory considering the peer-to-peer energy trading. *2020 2nd International Conference on Smart Power and Internet Energy Systems (SPIES)*, 322–326. https://doi.org/10.1109/SPIES48661.2020.9243067
17. Wang Z, Chen B, Wang J, et al. (2016) Networked microgrids for self-healing power systems. *IEEE Trans Smart Grid* 7: 310–319. https://doi.org/10.1109/TSG.2015.2427513
18. Chen C, Wang J, Ton D (2017) Modernizing distribution system restoration to achieve grid resiliency against extreme weather events: An integrated solution. *Proc IEEE* 105: 1267–1288. https://doi.org/10.1109/JPROC.2017.2684780
19. Ali AY, Hussain A, Baek JW, et al. (2021) Optimal operation of networked microgrids for enhancing resilience using mobile electric vehicles. *Energies* 14: 142. https://doi.org/10.3390/en14010142
20. Wang Y, Rousis AO, Strbac G (2021) A resilience enhancement strategy for networked microgrids incorporating electricity and transport and utilizing a stochastic hierarchical control approach. *Sustainable Energy Grids Netw* 26: 100464. https://doi.org/10.1016/j.segan.2021.100464
21. Teimourzadeh S, Tor OB, Cebeci ME, et al. (2019) A three-stage approach for resilience-constrained scheduling of networked microgrids. *J Mod Power Syst Clean Energy* 7: 705–715. https://doi.org/10.1007/s40565-019-0555-0
22. Tostado-Ve´liz M, Hasanien HM, Jordehi AR, et al. (2023) An interval-based privacy-aware optimization framework for electricity price setting in isolated microgrid clusters. *Appl Energy* 340: 121041. https://doi.org/10.1016/j.apenergy.2023.121041
23. Tostado-Ve´liz M, Kamel S, Aymen F, et al. (2022) A stochastic-IGDT model for energy management in isolated microgrids considering failures and demand response. *Appl Energy* 317: 119162. https://doi.org/10.1016/j.apenergy.2022.119162
24. Tostado-Ve´liz M, Hasanien HM, Jordehi AR, et al. (2023) Risk-averse optimal participation of a DR-intensive microgrid in competitive clusters considering response fatigue. *Appl Energy* 339: 120960. https://doi.org/10.1016/j.apenergy.2023.120960

25. Schneider KP, Radhakrishnan N, Tang Y, et al. (2019) Improving primary frequency response to support networked microgrid operations. *IEEE Trans Power Syst* 34: 659–667. https://doi.org/10.1109/TPWRS.2018.2859742
26. Miao Y, Hynan P, Jouanne AV, et al. (2019) Current li-ion battery technologies in electric vehicles and opportunities for advancements. *Energies* 12: 1074. https://doi.org/10.3390/en12061074
27. Mitali J, Dhinakaran S, Mohamad A (2022) Energy storage systems: A review. *Energy Storage Sav* 1: 166–216. https://doi.org/10.1016/j.enss.2022.07.002
28. Tian H, Qin P, Li K, et al. (2020) A review of the state of health for lithium-ion batteries: Research status and suggestions. *J Clean Prod* 261: 120813. https://doi.org/10.1016/j.jclepro.2020.120813
29. Rezvanizaniani SM, Liu Z, Chen Y, et al. (2014) Review and recent advances in battery health monitoring and prognostics technologies for electric vehicle (ev) safety and mobility. *J Power Sources* 256: 110–124. https://doi.org/10.1016/j.jpowsour.2014.01.085
30. Mit EV (2008) A guide to understanding battery specifications. Massachussetts Institute of Technology. Available from: http://web. mit. edu/evt/summary_battery_specifications. pdf.
31. Ma S, Jiang M, Tao P, et al. (2018) Temperature effect and thermal impact in lithium-ion batteries: A review. *Prog Nat Sci Mater Int* 28: 653–666. https://doi.org/10.1016/j.pnsc.2018.11.002
32. Jayasena KNC, Jayamaha DKJS, Lidula NWA, et al. (2019) SoC based multi-mode battery energy management system for dc microgrids. *2019 Moratuwa Engineering Research Conference (MERCon)*, 468–473. https://doi.org/10.1109/MERCon.2019.8818765
33. Pogaku N, Prodanovic M, Green TC (2007) Modeling, analysis and testing of autonomous operation of an inverter-based microgrid. *IEEE Trans Power Electron* 22: 613–625. https://doi.org/10.1109/TPEL.2006.890003
34. Ediriweera WS, Lidula N, Herath HDB (2023) Robust microgrids for distribution systems with high solar photovoltaic penetration. *Arch Electr Eng* 72: 785–809. http://dx.doi.org/10.24425/aee.2023.146050
35. Guo X, Guo H (2011) Simulation and control strategy of a micro-turbine generation system for grid connected and islanding operations. *Energy Proc* 12: 368–376. https://doi.org/10.1016/j.egypro.2011.10.050
36. Shao W, Wu R, Ran L, et al. (2020) A power module for grid inverter with in-built short-circuit fault current capability. *IEEE Trans Power Electron* 35: 10567–10579. https://doi.org/10.1109/TPEL.2020.2978656
37. Pan C, Tao S, Fan H, et al. (2021) Multi-objective optimization of a battery-supercapacitor hybrid energy storage system based on the concept of cyber-physical system. *Electronics* 10: 1801. https://doi.org/10.3390/electronics10151801
38. Naseri F, Farjah E, Allahbakhshi M, et al. (2017) Online condition monitoring and fault detection of large supercapacitor banks in electric vehicle applications. *IET Electr Sys Transp* 7: 318–326. https://doi.org/10.1049/iet-est.2017.0013
39. Yang H (2018) Estimation of supercapacitor charge capacity bounds considering charge redistribution. *IEEE Trans Power Electron* 33: 6980–6993. https://doi.org/10.1109/TPEL.2017.2764423
40. Kalbitz R, Puhane F (2022) Supercapacitor—A guide for the design-in process. Wurth Elektronik, *Tech Rep*. Available from: https://www.we-online.com/en/support/knowledge/application-notes?d=anp077-supercapacitor.

41. Qoria T, Cossart Q, Li C, et al. (2018) Wp3-control and operation of a grid with 100% converter-based devices. deliverable 3.2: Local control and simulation tools for large transmission systems. H2020 MIGRATE project. Available from: https://www. h2020-migrate. eu, 2018.
42. Paquette AD, Divan DM (2015) Virtual impedance current limiting for inverters in microgrids with synchronous generators. *IEEE Trans Ind Appl* 51: 1630–1638. https://doi.org/10.1109/TIA.2014.2345877
43. Behabtu HA, Messagie M, Coosemans T, et al. (2020) A review of energy storage technologies' application potentials in renewable energy sources grid integration. *Sustainability* 12: 10511. https://doi.org/10.3390/su122410511
44. Georgious R, Refaat R, Garcia J, et al. (2021) Review on energy storage systems in microgrids. *Electronics* 10: 2134. https://doi.org/10.3390/electronics10172134
45. Wang H, Blaabjerg F (2014) Reliability of capacitors for dc-link applications in power electronic converters—An overview. *IEEE Trans Ind Appl* 50: 3569–3578. https://doi.org/10.1109/TIA.2014.2308357
46. Susanto J, Shahnia F, Ghosh A, et al. (2014) Interconnected microgrids via back-to-back converters for dynamic frequency support. *2014 Australasian Universities Power Engineering Conference (AUPEC)*, 1–6. https://doi.org/10.1109/AUPEC.2014.6966616
47. Worku MY, Hassan MA, Abido MA (2019) Real time energy management and control of renewable energy based microgrid in grid connected and island modes. *Energies* 12: 276. https://doi.org/10.3390/en12020276
48. Chakraborty S, Kramer B, Kroposki B (2009) A review of power electronics interfaces for distributed energy systems towards achieving low-cost modular design. *Renewable Sustainable Energy Rev* 13: 2323–2335. https://doi.org/10.1016/j.rser.2009.05.005
49. Blaabjerg F, Chen Z, Kjaer S (2004) Power electronics as efficient interface in dispersed power generation systems. *IEEE Trans Power Electron* 19: 1184–1194. https://doi.org/10.1109/TPEL.2004.833453
50. Pawel S (2014) Matrix converter interfaces two three-phase AC systems as a component of smart-grid. *2014 International Symposium on Power Electronics, Electrical Drives, Automation and Motion*, 683–688. https://doi.org/10.1109/SPEEDAM.2014.6872047
51. Carvalho EL, Blinov A, Chub A, et al. (2022) Grid integration of dc buildings: Standards, requirements and power converter topologies. *IEEE Open J Power Electron* 3: 798–823. https://doi.org/10.1109/OJPEL.2022.3217741
52. Yuan Y, Chang L, Song P (2007) A new front-end converter with extended hold-up time. *2007 Large Engineering Systems Conference on Power Engineering*, 275–278. https://doi.org/10.1109/LESCPE.2007.4437392
53. Electromagnetic compatibility part 4–11: Testing and measurement techniques voltage dips, short interruptions and voltage variations immunity tests. *International Electrotechnical Commission, Geneva,Switzerland, Standard IEC 61000-4-11:2020, 2020*. Available from: https://webstore.iec.ch/publication/63503.
54. IEEE standard for the specification of microgrid controllers. *IEEE*, 1–43, 2018. https://doi.org/10.1109/IEEESTD.2018.8340204
55. IEEE standard for interconnection and interoperability of distributed energy resources with associated electric power systems interfaces. IEEE Std 1547-2018 (Revision of IEEE Std 1547-2003), 1–138, 2018. https://doi.org/10.1109/IEEESTD.2018.8332112

56. Anderson WW (2020) Resilience assessment of islanded renewable energy microgrids. Available from: https://apps.dtic.mil/sti/citations/AD1126753.
57. Ediriweera WEPS, Lidula NWA (2023) Adaptive load shedding technique for energy management in networked microgrids. *2023 IEEE 17th International Conference on Industrial and Information Systems (ICIIS)*, 465–470. https://doi.org/10.1109/ICIIS58898.2023.10253509
58. Ediriweera WEPS, Lidula NWA (2023) Adaptive droop controller for energy management of islanded AC microgrids. *2023 Moratuwa Engineering Research Conference (MERCon)*, 292–297. http://dx.doi.org/10.1109/MERCon60487.2023.10355428

Supplementary

Table 7. Impedance of the cables.

Microgrid	Cable[a]	Resistance(mΩ)	Inductance(μH)	Capacitance(μF)
1	Cable 1-2	70.5	99	0.105
	Cable 2-3	7.50	99	0.105
2	Cable 1-2	155	163	0.122
	Cable 2-3	15.552	163	0.112
3	Cable 1-2	173	182	0.124
	Cable 2-3	17.39	182	0.124
4	Cable1-2	173	182	0.124
	Cable 2-3	17.39	182	0.124
n/a	Cable 1	333	351	0.239
n/a	Cable 2	100	105	0.721
n/a	Cable 3	257	271	0.185
n/a	Cable 4	333	351	0.239

[a]Cable i-j represents the cable connecting i and j bus bars in the considered microgrids, and cable k represents the interconnecting cables

Table 8. Parameters of the test system.

MG/ SW	$P_{L,peak}$ (MW)	$P_{C,rec}$ (MW)	$P_{C,max}$ (MW)	P_{rated_b} (MW)	C_d (mF)	k	P_c (MW)	C_s (F)	R_s (Ω)	P_{MG} (MW)	P_{cable} (MW)	P_{rated_SW} (MW)	t_{hold} (ms)	C_{DC} (mF)
1	4.51	6.8	9	12.75	16	0.071	27	4.4	0.370	2.05	1	2.12	50	18
2	0.58	1	2	2.82	4	1.46	5.59	0.9795	1.4	1	1	2.12	50	18
3	2.2	3.3	4.4	6.22	8	0.23	13.17	2.15	0.780	1	1	2.12	50	18
4	3.4	5.1	6.8	9.61	12	0.125	20	3.3	0.502	1.7	1.7	3.6	60	35